Journal of Materials Chemistry A

ROYAL SOCIETY OF CHEMISTRY

PAPER

View Article Online
View Journal

Cite this: DOI: 10.1039/d5ta10332k

Supercapacitor-based CO_2 capture enhanced by electrolyte pH control

Selina E. Wiesner, [ab] Zeke Coady, [b] Zhen Xu, [c] Malina Seyffertitz [b] and Alexander C. Forse *[b]

Received 18th December 2025
Accepted 2nd April 2026

DOI: 10.1039/d5ta10332k

rsc.li/materials-a

Supercapacitive swing adsorption (SSA) is emerging as an energy-efficient alternative to traditional thermally-driven CO_2 capture technologies. While a range of operational factors have been actively explored to increase understanding of this technology, SSA is currently constrained by low CO_2 capture rates. In this work, we investigate how electrochemical CO_2 capture responds to changes in electrolyte pH by combining galvanostatic CO_2 adsorption measurements with quantitative solid-state ^{13}C-NMR spectroscopy. Our measurements show 30% higher adsorption rates for basic electrolytes than for neutral electrolytes. In contrast, in an acidic electrolyte, we see substantially lower adsorption rates and capacities. To probe the origin of these observations, we use ^{13}C NMR spectroscopy on uncharged electrolyte-soaked electrodes to examine CO_2 speciation. While dissolved CO_2 is detected across all electrolytes, bicarbonate concentrations increase with increasing initial electrolyte pH (*i.e.* the pH), before any reaction-induced pH changes occur, suggesting a bicarbonate- or pH-swing driven mechanism. Overall, our study provides additional insights into the factors governing CO_2 capture in SSA by highlighting the role of CO_2 speciation and electrolyte pH in optimising device performance.

Introduction

Climate change, driven by excessive CO_2 emissions from fossil fuels and industrial activities, poses a critical threat to ecosystems and societies worldwide.[1] While global efforts like the Paris Agreement aim to limit warming to below 1.5 °C compared to pre-industrial levels and reach net-zero emissions by 2050, many sectors remain dependent on fossil fuels.[2,3] The situation has even escalated further: in 2024, a 1.6 °C rise in global temperature (12 month average) was reported compared to the beginning of the last century.[4] Consequently, carbon capture technologies, including point-source capture from industrial flue gas and direct air capture (DAC) from the atmosphere, are crucial for complementing emission reduction strategies and achieving climate goals.[5]

Amine scrubbing, a mature carbon capture technology, involves amines reacting with CO_2 to form carbamates. This technology benefits from fast absorption and high CO_2 selectivity.[6] To release the CO_2, however, a large amount of energy is required to reverse the process, typically through temperature- or pressure-swing.[6] In this context, the advent of electrochemical CO_2 capture technologies has demonstrated the potential for increased efficiency, stability, and safety over the state-of-the-art amine capture approach.[7,8] Examples for electrochemical carbon capture methods use redox-active molecules like quinones that reversibly bind CO_2 [9,10] or employ electrochemically-mediated pH swings using phenazine-based molecules.[11] By integrating electrochemical carbon capture technologies with renewable energy sources, it is possible to create a sustainable, closed-loop system that captures CO_2 while minimising the environmental footprint of the technologies.[12]

Supercapacitive swing adsorption (SSA) is a particularly promising electrochemical carbon capture technology.[13] In SSA, CO_2 is adsorbed when charging an electric double-layer capacitor (EDLC), and is subsequently desorbed when discharging the device. Typically, in SSA setups, the working electrode is preferentially exposed to a gas reservoir (Fig. 1a). A key advantage of SSA lies in its utilisation of low-cost, earth-abundant carbon electrode materials and environmentally friendly aqueous electrolytes.[13] Furthermore, as charge storage takes place electrostatically in EDLCs, the devices exhibit high cyclability, capable of undergoing over 10 000 charge–discharge cycles without significant degradation.[14] However, SSA is limited by its low CO_2 adsorption rate (100–500 mmol kg^{-1} h^{-1}), which is outperformed by other electrochemical CO_2 capture processes.[15,16] This is partly due to its low capacity (typically around 100 mmol kg^{-1}, normalised to the mass of the working electrode when using commercial activated carbon electrodes)[17] compared with amine-based capture

[a]Faculty of Chemistry and Pharmacy, Ludwig-Maximilians-Universität München, Munich 81377, Germany

[b]Yusuf Hamied Department of Chemistry, University of Cambridge, Cambridge CB2 1EW, UK. E-mail: acf50@cam.ac.uk

[c]Department of Materials and Henry Royce Institute, University of Manchester, Oxford Rd, Manchester M13 9PL, UK

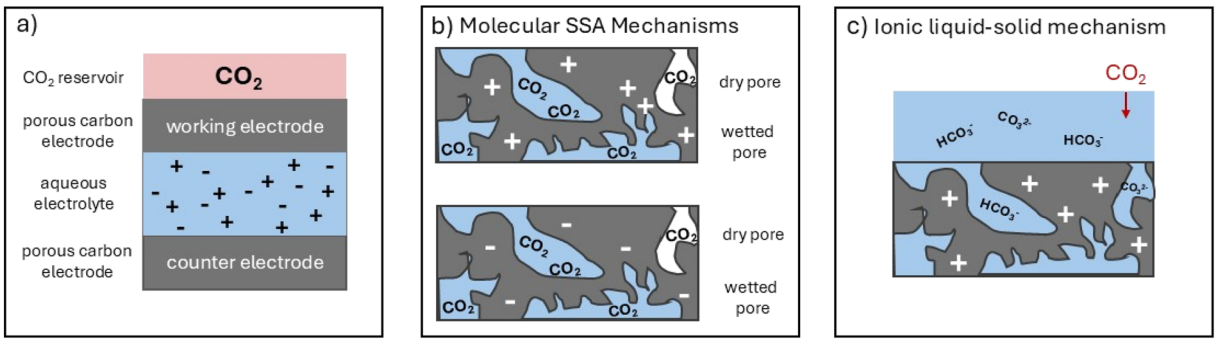

Fig. 1 (a) Typical setup of a supercapacitor used for supercapacitive swing adsorption. The working electrode is exposed to a CO_2-containing reservoir and can be charged negatively (negative charging mode) or positively (positive charging mode). (b) Molecular mechanisms of CO_2 capture visualised for the carbon electrode only. Adsorption of CO_2 within dry or wetted pores of the porous carbon electrode; mechanisms are polarity-independent and can occur at both the negatively and positively charged electrode. (c) Ionic mechanism of CO_2 capture: CO_2 from the reservoir dissolves in the aqueous electrolyte, creating bicarbonate and carbonate ions. Adsorption of CO_2-derived ionic species (HCO_3^- or CO_3^{2-}) at the positively charged electrode.

technologies (800 mmol kg^{-1}), but may also be limited by other factors, such as gas–liquid mass transfer. Additionally, the underlying adsorption mechanism is poorly understood, hindering the rational design of SSA devices with improved CO_2 adsorption capacities.[15]

To increase the CO_2 adsorption capacities of the devices, the electrolyte composition,[18] the electrolyte concentration,[19] the physicochemical properties of the activated carbon electrodes,[20–22] the operating voltage windows,[23] the charging protocols,[24] the use of different materials for the counter electrode,[25] and the polarity of the gas-exposed electrode[17] have been investigated. All these studies have shown that tuning specific system parameters can lead to higher adsorption capacities; however, more rational process optimisation is limited by a poor understanding of the mechanism of action.[20,26]

Zhu *et al.* originally proposed three CO_2 capture mechanisms, differentiated by the species involved in capture – molecular CO_2 *versus* CO_2-derived ions such as bicarbonate and carbonate.[19] Fig. 1 introduces the molecular and ionic mechanisms of capture. The molecular mechanism suggests that neutral CO_2 molecules are captured in electrolyte-filled (or non-infiltrated) pores of the activated carbon electrode during charging of the supercapacitor (Fig. 1b). As the CO_2 molecule is neutral, capture can happen at the counter electrode regardless of its polarity.

A recent study demonstrated the feasibility of this mechanism, showing that the presence of CO_2 in the EDL formed on gold electrodes immersed in aqueous electrolytes decreases capacitance.[27] However, these molecular mechanisms do not fully account for the experimental observations reported by Binford *et al.* for activated carbon electrodes, where CO_2 capture and release depend on electrode polarity.[17] While it is possible in principle for a molecular mechanism to exhibit polarity dependence, the specific mechanism illustrated in Fig. 1b would be expected to lead to CO_2 adsorption irrespective of electrode polarity. The experimentally observed polarity-dependent behaviour therefore suggests that additional factors beyond this molecular mechanism must be contributing to the observed behaviour.

In the ionic liquid–solid mechanism (Fig. 1c), bicarbonate (or carbonate) plays a major role in CO_2 capture and release, as CO_2 capture and release are driven by the electro-sorption of CO_2-derived ionic species into the electrical double layer, which influences the underlying chemical equilibria shown in eqn (1)–(4).[17,19,20]

$$CO_{2(g)} \rightleftharpoons CO_{2(aq)} \quad (1)$$

$$CO_{2(aq)} + H_2O_{(l)} \rightleftharpoons H_2CO_{3(aq)} \quad (2)$$

$$H_2CO_{3(aq)} + H_2O_{(l)} \rightleftharpoons HCO_3^-{}_{(aq)} + H_3O^+{}_{(aq)} \quad (3)$$

$$HCO_3^-{}_{(aq)} + H_2O_{(l)} \rightleftharpoons CO_3^{2-}{}_{(aq)} + H_3O^+{}_{(aq)} \quad (4)$$

Previous studies based on electrochemical CO_2 capture measurements and COMSOL modelling proposed that charging the gas-facing electrode negatively results in local depletion of HCO_3^-, promoting CO_2 capture; the reverse effect occurs upon positive charging.[17,20,26] Recently, two preprints have also proposed a pH swing-driven mechanism of CO_2 capture, with one showing that use of a cation-exchange membrane may enhance SSA by stabilising a high-pH region at the gas-facing electrode.[28,29] This emerging pH-swing hypothesis likely involves pH changes bulk of the electrolyte upon charging and discharging of the supercapacitor and requires further experimental proof involving *in operando* pH monitoring.

It has also been hypothesised that both the molecular and the ionic liquid–solid mechanism can occur and that the degree to which each of them contributes to CO_2 storage depends on the characteristics of the system, including electrolyte properties (*e.g.*, pH, ionic species, concentration) and electrode structures (*e.g.*, porosity, disorder, functionality).[27]

Overall, electrolyte pH emerges as a central factor linking CO_2 speciation, adsorption behaviour, and capture performance. Motivated by this, we investigate the electrochemical CO_2 adsorption behaviour of activated carbon electrodes in a 1 M Na_2SO_4 electrolyte across a range of pH values, including

strongly acidic, neutral, and alkaline conditions. The reported pH values correspond to the initial pH measured prior to electrochemical testing, as the final pH during and after electrochemical testing could not be reliably determined. We combine this with quantitative solid-state nuclear magnetic resonance (ss-NMR) measurements of the electrode/electrolyte/$^{13}CO_2$ system[30] (without charging) to probe CO_2 speciation within the electrolyte at varying pH. These results reveal that increasing the electrolyte pH results in higher rates of SSA capture, correlating with increased bicarbonate formation; in contrast, decreasing pH results in lower capacities and rates of SSA capture, as well as the absence of bicarbonate formation. Our results, therefore, reveal clear pH-dependent changes in speciation that influence capture performance, supporting the view that SSA is governed by ionic pathways or a pH-swing-driven mechanism.

Results

Effects of different electrolyte pH on CO_2 capture performance

To investigate the impacts of electrolyte pH on electrochemical CO_2 capture performance, we employed an activated carbon electrode (YP80F) and 1 M Na_2SO_4 electrolyte with different pH values as benchmark materials. We prepared acidic ($pH_{initial}$ 1.1), neutral ($pH_{initial}$ 7.0), and basic ($pH_{initial}$ 13.4) electrolytes, assembled a symmetric coin-cell supercapacitor (meaning mass-identical carbon electrodes) with a meshed top case. Starting from the initial electrolyte pH (pH_{inital}), the electrolyte pH inside the coin cell is expected to change as the system equilibrates (*e.g.* exposed to the experimental conditions of the SSA measurements). First, interactions between the electrolyte and the porous carbon electrodes modify pH_{inital} as the electrolyte equilibrates with surface functional groups of the porous activated carbon and its point of zero charge (Fig. S9a).[31] In addition, diffusion of CO_2 from a fixed reservoir into the electrolyte results in further acidification. Because the coin cell supercapacitors are a sealed system for the purpose of our CO_2 uptake measurements, direct *in situ* measurement of the final electrolyte pH (pH_{final}) is challenging. Instead, the pH was measured after opening coin cells after their exposure to experimental SSA conditions. Based on these measurements, the initially acidic electrolyte is estimated to be approximately 1.3, the initially neutral electrolyte 8.4, and the initially basic electrolyte 9.6. As this work focuses on the overall influence of electrolyte pH on SSA, pH values are reported with respect to the initial electrolyte pH (pH_{inital}) throughout the manuscript unless stated otherwise. The coin-cell type supercapacitor was introduced into a "gas cell" (Fig. 2a), which was custom-designed in our laboratory for the SSA work.[17,20,25,26] Within the "gas cell", the meshed coin-cell type supercapacitor is exposed to a pure CO_2 headspace, and any changes in pressure (from adsorption or desorption) are monitored using in-built pressure transducers. This setup allows simultaneous pressure recording while charging and discharging the supercapacitor at constant current (galvanostatic charge and discharge). In this work, we employ two different charging protocols, the negative and the positive charging mode. In the negative charging mode, the gas-exposed electrode is charged negatively to −0.8 V, followed by a 5 minute voltage hold at −0.8 V before discharging the cell to 0.0 V. In the positive charging mode, the gas-facing electrode is charged to +0.8 V, held at +0.8 V for 5 minutes, and subsequently discharged to 0.0 V again. The negative or positive charging modes, therefore, refer to the polarisation of the gas-exposed electrode, identified as negative or positive, respectively. As the pressure transducers are not selective for monitoring CO_2 (over other gases), the overall pressure development inside the gas cells was carefully monitored to account for any continuous and irreversible pressure changes during charging and discharging of the supercapacitor. Parasitic side reactions (*e.g.*, water splitting) that would increase pressure are ruled out by the overall high coulombic efficiency (Fig. S1) and the lack of an irreversibly increasing baseline pressure (Fig. S2). In our systems, continuous pressure changes have been previously attributed to corrosion within the coin cells, especially at low current densities (10–50 mAg^{-1}).[25,26] At higher current densities, the pressure baseline stabilises, enabling reliable determination of CO_2 uptake. Therefore, this work investigates the CO_2 uptake at high current densities (100, 150 and 300 mAg^{-1}).

To test the impact of different electrolyte pH on electrochemical CO_2 capture behaviour, we employed the negative charging mode to the assembled supercapacitor cells containing different electrolyte pH and exposed them to a pure CO_2 gas headspace. For all three electrolyte pH values, CO_2 capture is observed upon negative charging, visible by a decrease in pressure (Fig. 2b–d). In the positive charging mode, supercapacitors release CO_2 during charging, as indicated by an increase in pressure (Fig. S3). In essence, the supercapacitor cell captures CO_2 when the gas-exposed electrode receives electrons across all tested pH values of the electrolyte. These observations agree with previously conducted experiments employing different activated carbons as electrodes[20,26] or other electrolytes.[17]

Excitingly, the pH of the electrolyte affects the magnitude of pressure changes observed across all measured pH values when the negative charging mode is employed. When we compare the acidic system (Fig. 2c) to the neutral benchmark system (Fig. 2b, Δp ~5 mbar), we see that the acidic system exhibits a smaller change in pressure(Δp < 5 mbar), suggesting that less CO_2 is captured. In contrast, the basic system (Fig. 2d) displays a higher pressure change (Δp ~10 mbar) than the neutral reference. To confirm this initially observed qualitative change, a comprehensive quantitative analysis of CO_2 capture and the involved speciation using ss-NMR spectroscopy will be presented in the following section of this work.

Quantitative ss-NMR reveals CO_2-derived speciation within electrolyte-soaked electrodes

While the effects of solution pH on CO_2 uptake and speciation in bulk solution are very well-established, these properties are much more complex in electrode/electrolyte systems due to the possibility of nanoconfinement-induced oversolubility and changes to reactivity.[30,32]

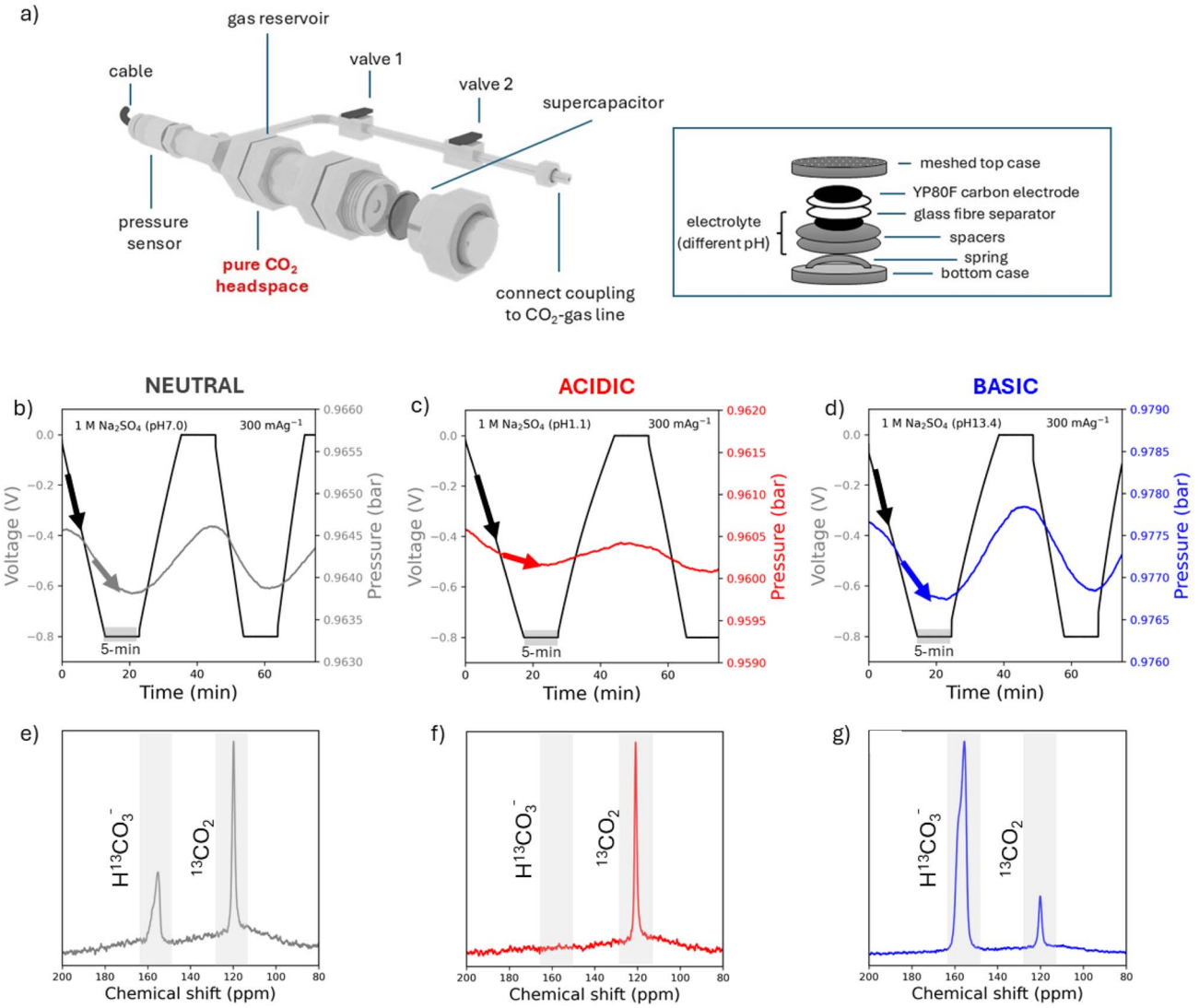

Fig. 2 CO_2 capture behaviour during negative charging mode for all measured electrolyte pH. (a) Experimental gas cell setup for electrochemical CO_2 sorption measurements and supercapacitor coin cell stacking sequence with meshed top case. Voltage-pressure curves for (b) neutral $pH_{initial} = 7.0$ (grey), (c) acidic $pH_{initial} = 1.1$ (red) and (d) basic $pH_{initial} = 13.4$ (blue) Na_2SO_4 electrolyte, with cells using YP80F electrodes and a pure CO_2 gas headspace. The coin-cell type supercapacitors were inserted into the gas cell and charged to −0.8 V, followed by a 5 min voltage hold and subsequent discharge to 0.0 V. ^{13}C ss-NMR (9.4 T, 5 kHz MAS) measurements on electrolyte/electrode/$^{13}CO_2$ systems to investigate the CO_2-derived speciation inside the (e) acidic (f) neutral and (g) basic electrolyte.

As stated previously, it is challenging to determine the pH_{final} of the electrolyte *in situ* without disassembly of the experimental setup. To explore how the change in electrolyte pH affects the CO_2 speciation in the activated carbon/electrolyte system, we therefore performed quantitative ss-NMR measurements of the electrolyte-soaked YP80F activated carbon thin film in a $^{13}CO_{2(g)}$ dosed NMR-rotor, modelling the state of an SSA module without charging the cell. Our NMR experiment circumvents the challenges of direct pH_{final} measurements in the carbon-electrolyte system and allows us to directly probe the effects of pH_{inital} on SSA performance. In the ^{13}C NMR spectrum of the neutral benchmark system (Fig. 2e), NMR resonances are observed for both CO_2 (at 120 ppm) and HCO_3^- (at 155 pm). The 120 ppm peak was assigned to $CO_{2(aq)}$ inside the activated carbon pores, which is shifted to a lower frequency from the literature value of 125–126 ppm for $CO_{2(aq)}$[33–35] due to a nucleus-independent chemical shift (NICS) effect driven by confinement inside the activated carbon's pores.[31,36] In-pore $CO_{2(g)}$ is not believed to be present, based on comparison to a reference spectrum of dry YP80F dosed with $^{13}CO_{2(g)}$ showing higher uptake and a different chemical shift in the dry sample (Fig. S4). Similarly, the peak at 155 pm corresponds to $HCO_3^-{}_{(aq)}$ inside the activated carbon pores, again shifted to a lower frequency from the literature value of 160–161 ppm by the NICS effect.[35,37] Estimating the $HCO_3^-{}_{(aq)}$:$CO_3^{2-}{}_{(aq)}$ equilibrium *via* the chemical shift (after accounting for the NICS effect) indicates that there is negligible $CO_3^{2-}{}_{(aq)}$ in the system.[37,38] An additional shoulder peak is observed at 158 ppm, which likely reflects a $HCO_3^-{}_{(aq)}$ exchange environment between the surface of the activated

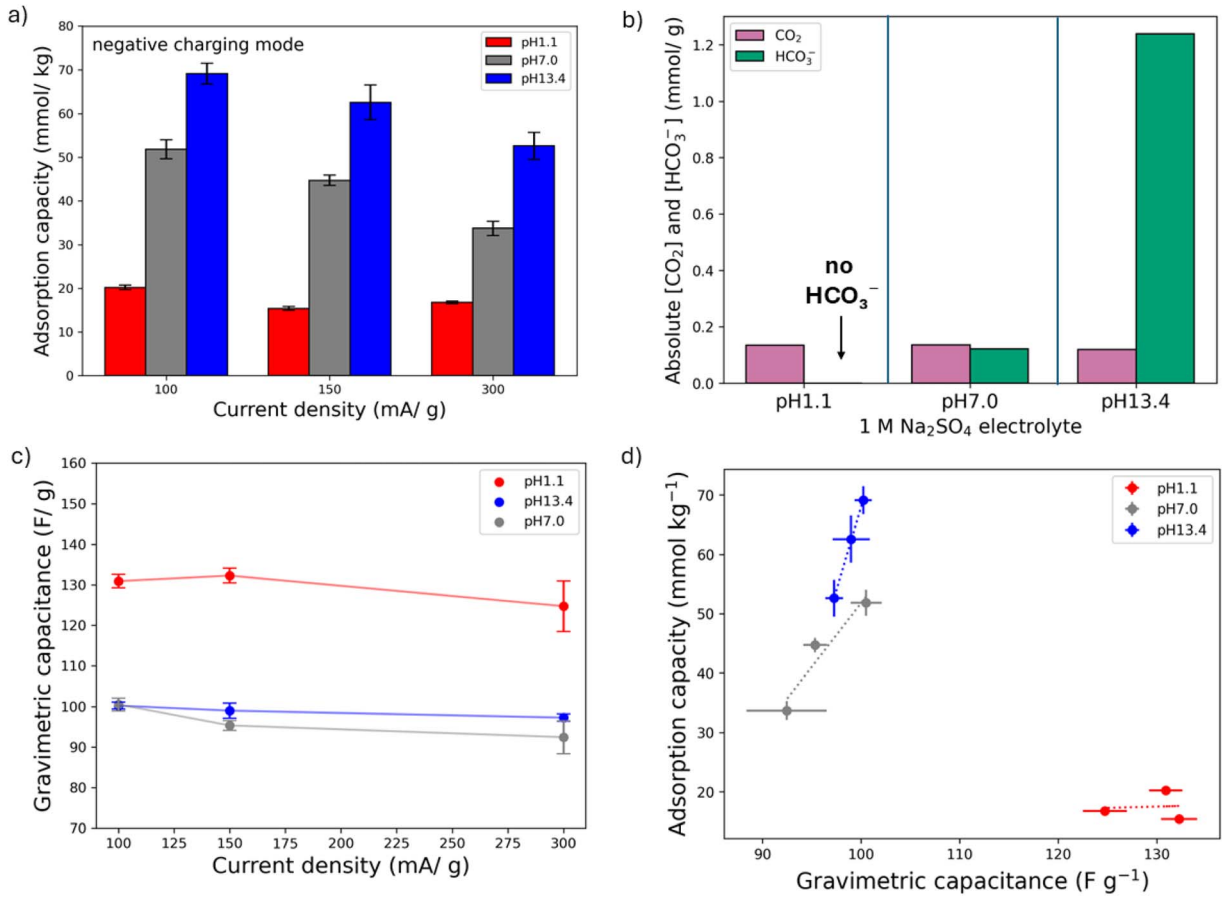

Fig. 3 (a) Adsorption capacities at different current densities for the YP80F/Na_2SO_4 system (acidic, neutral and basic electrolyte pH) in the negative charging mode. In these experiments, the supercapacitor was charged to −0.8 V, followed by a 5 min voltage hold and a discharge step to 0 V. Measured for three current densities (100, 150, 300 mA g^{-1}). Error bar calculated as the standard deviation from 5 cycles measured for every current density. For reproducibility purposes, two independent coin cells were assembled by the same researcher and measured in different gas cell setups (Fig. S5). (b) Gravimetric uptake of CO_2 and HCO_3^- in model uncharged SSA systems, calculated from NMR integrations. Uptake is normalised to the mass of activated carbon. The standard deviation divided by the mean was 5.6% for moles of CO_2 and 7.2% for moles of HCO_3^-. (c) Gravimetric capacitances calculated from the discharge step of constant current measurements, excluding the voltage drops. (d) Correlations and linear fits between the gravimetric capacitance (F g^{-1}) and adsorption capacity (mmol kg^{-1}) for acidic, neutral, and basic electrolytes.

carbon and the electrolyte bulk.[39] Further discussion of peak assignment is contained inside the SI.

In the ^{13}C NMR spectrum of the acidic electrolyte system (Fig. 2f), only the $CO_{2(aq)}$ peak at 120 ppm is observed, indicating that HCO_3^- formation has been suppressed. Meanwhile, in the basic electrolyte system (Fig. 2g), formation of significantly more $HCO_3^-{}_{(aq)}$ is observed compared to the neutral system. No change is observed in the $HCO_3^-{}_{(aq)}$ peak's chemical shift, indicating that $CO_3^{2-}{}_{(aq)}$ content remains negligible. In a bulk system, this corresponds to a pH below 10, compared to our starting point of 13.4 (based on CO_2 in pure water, Fig. S5). We attribute this to a combination of two effects: first, the activated carbon/1 M $Na_2SO_{4(aq)}$ system has a pH_{pzc} of 9.1 (Fig. S9), indicating that contact with the carbon reduces the pH of the basic electrolyte; and second, dissolution of CO_2 further acidifies the solution.

Overall, quantitative ss-NMR experiments indicate that altering the electrolyte pH primarily affects HCO_3^- in the electrode/electrolyte system: acidic electrolyte suppresses bicarbonate formation, while basic electrolyte favours it. In contrast, CO_2 uptake is less affected by pH.

In order to assess how the initial CO_2 speciation and uptake might explain the observed changes in SSA performance, we compared the "electrochemical CO_2 capacity" (Fig. 3a) and the "initial CO_2 and HCO_3^- uptake" in our uncharged model SSA electrodes (Fig. 3b), which were calculated from NMR peak integrations through comparison to quantitative ^{13}C NMR of samples with known CO_2 uptake (see SI calculations). A large increase in electrochemical CO_2 capture capacity is observed as the electrolyte pH is increased, regardless of the current density (Fig. 3a). At the same time, electrolyte pH increases are accompanied by significant changes in initial CO_2 speciation and uptake measured by NMR spectroscopy (Fig. 3b). From NMR we observe that the initial amount of $CO_{2(aq)}$ present is consistently 0.11–0.13 mmol g^{-1} across all three systems, while the amount of bicarbonate varies from 0 mmol g^{-1} in the acidic system to 1.2 mmol g^{-1} in the basic system. The increase in "electrochemical CO_2 capacity" with increasing initial

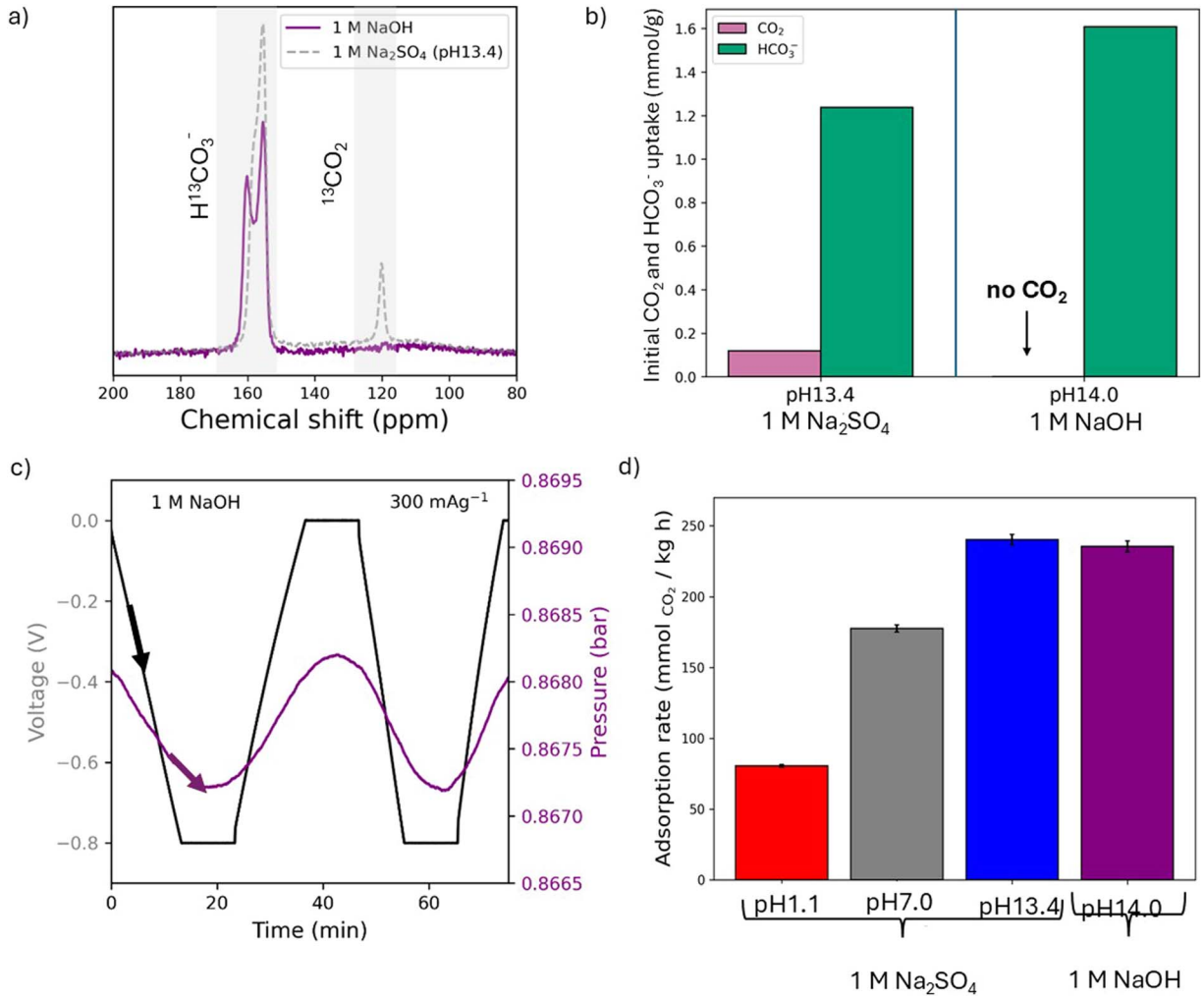

Fig. 4 (a) ^{13}C ss-NMR measurement on the YP80F/NaOH/$^{13}CO_2$ system (dosed at 10 psi), with the analogous spectrum for basic (pH initial 13.4) 1 M $Na_2SO_{4(aq)}$ electrolyte plotted for comparison in grey. (9.4 T ssNMR, 5 kHz MAS) (b) pressure voltage curves of SSA in 1 M NaOH in the negative charging mode. (c) Comparison between CO_2 and bicarbonate concentration for basic 1 M Na_2SO_4 and 1 M NaOH electrolyte. (d) Overall adsorption rates ($mmol_{CO_2}$ kg^{-1} h^{-1}) for all the measured electrolyte systems in this work at 300 mAg^{-1}.

bicarbonate concentration suggests that bicarbonate plays a key role in CO_2 capture in aqueous based supercapacitors. With regards to the proposed mechanisms within the literature, the ionic liquid–solid mechanism as well as a pH-swing dominated mechanism become more likely as they are directly or indirectly influenced by bicarbonate concentration. Work is ongoing to further demonstrate this effect, and identify a mechanistic explanation of how increasing bicarbonate concentration leads to enhanced CO_2 capture in SSA systems. Interestingly, when performing an SSA experiment in 1 M $NaHCO_3$ (Fig. S10), similar CO2 adsorption capacities were obtained compared to measurements obtained with basic 1 M Na_2SO_4 ($pH_{initial} = 13.4$) (Fig. S10). Both electrolytes exhibit comparable CO_2 adsorption performance, with no significant difference observed between them. This result indicates that the presence of bicarbonate ions plays a key role in the SSA mechanism, while variations in pH primarily influence the ionic speciation and concentration rather than fundamentally altering the adsorption behaviour. The similarity in performance between the two electrolytes therefore supports the conclusion that bicarbonate-related equilibria, rather than pH alone, govern the observed CO_2 uptake behaviour.

Enhanced SSA uptake in basic systems is not explained by changes in capacitance

Throughout the literature, a positive correlation between the electrochemical capacitance of the activated carbon electrodes and adsorption capacity has been reported.[21,22] However, in this work, the acidic system shows the highest electrochemical capacitance (132.3 ± 1.8 F g^{-1} at 150 mA g^{-1}) while the basic and neutral systems show a similar capacitance around 100 F g^{-1} (Fig. 3c). The enhanced capacitance of the acidic system can be attributed to the activation of functional groups (*e.g.*, quinones) on the activated carbon's surface at low pH, which facilitates faradaic charge storage. In contrast, higher pH levels diminish this effect and reduce capacitance.[40–42] Our results do not follow the trend of higher electrochemical CO_2 capture for

electrodes with increased capacitance,[21,22] as the acidic system shows the highest electrochemical capacitance but the smallest electrochemical CO_2 adsorption capacity (Fig. 3d). To further investigate this relationship, electrochemical CO_2 capacities were plotted against the gravimetric capacitances (Fig. 3d). Indeed, there is no linear correlation among the acidic, neutral, and basic systems visible, suggesting that the relationship between electrochemical CO_2 capacity and capacitance is not straightforward and is further influenced by CO_2 speciation within the electrolyte. In particular, recent studies have shown that the presence of molecular CO_2 in the electrolyte/the electric double layer can indeed modify electrochemical capacitance.[27,43,44] Additionally, the presence of carbonate/bicarbonate may also contribute to a change in EDL structure/charge storage. Some supercapacitors using mixed ion electrolytes have been shown to have an increased capacitance due to a change in packing arrangements within the EDL.[45] Our results highlight the significant role of electrolyte speciation in influencing both the charge storage behaviour of supercapacitors and the capacity for CO_2 adsorption. Additionally, the overall similar charge storage kinetics observed for all electrolytes suggest that other physicochemical properties (*e.g.*, ionic conductivity) do not play a dominant role in the charging behaviour under the conditions studied. Further research is necessary to clarify the relationships between these parameters.

Basic electrolytes show higher CO_2 uptake rates

To further probe the role of electrolyte pH on SSA modules, and to control for potential competition between HCO_3^- and SO_4^{2-} electrosorption during charging, we also examined 1 M NaOH ($pH_{initial}$ 14.0, pH_{final} 12.3) electrolyte. NMR measurements revealed that in the $^{13}CO_2$/YP80F/1 M NaOH system, bicarbonate is the sole CO_2-derived species present in the electrolyte (Fig. 4a), with no $CO_{2(aq)}$ and minimal $CO_3^{2-}{}_{(aq)}$ present. Fig. 4b compares NMR-derived uptake and speciation inside the basic Na_2SO_4 and the 1 M NaOH electrolyte/electrode systems. Integration indicates the formation of approximately 30% more bicarbonate in the NaOH ($pH_{initial}$ 14) system compared to the basic ($pH_{initial}$ 13.4) Na_2SO_4 electrolyte, which is likely driven by the higher OH^- concentration prior to contact with CO_2. Across all current densities and charging modes, the CO_2 adsorption capacities for the NaOH electrolyte are slightly lower than those measured for the basic Na_2SO_4 electrolyte ($pH_{initial}$ 13.4) (Fig. 3a). It is evident that the higher bicarbonate concentration does not further increase adsorption capacity, indicating the limitations of increasing the system's adsorption capacity and suggesting that the presence or absence of SO_4^{2-} has little effect on SSA activity.

Achieving high adsorption capacities during SSA is an important goal, but ultimately, high CO_2 adsorption rates are more relevant for the development and industrial scaling of SSA technology. Generally, higher adsorption rates can be achieved by applying current densities above 100 mAg^{-1}, and we therefore prioritised such current densities in our study. Previous research indicates that the SSA adsorption capacity significantly declines at higher current densities, primarily due to kinetic limitations.[20,24,26] Amongst all the investigated electrolytes in this study, the basic Na_2SO_4 electrolyte ($pH_{initial}$ 13.4) shows the highest adsorption rates at the current density of 300 mA g^{-1} (Fig. 4d). With 240 $mmol_{CO_2}$ kg^{-1} h^{-1}, the adsorption rate is 35% higher in comparison to the neutral electrolyte (177 $mmol_{CO_2}$ kg^{-1} h^{-1}, pH initial 7.0) and approximately three times higher than the acidic electrolyte (80 $mmol_{CO_2}$ kg^{-1} h^{-1}, $pH_{initial}$ 1.1). It becomes evident that the basic electrolyte systems (1 M NaOH and $pH_{initial}$ 13.4 Na_2SO_4) examined here demonstrate particularly strong performance at elevated current densities, suggesting that basic electrolytes (where bicarbonate species dominate) show improved kinetics.

Conclusion

By performing CO_2 capture in electrolytes with variable pH levels, we investigated the effects of pH on supercapacitive swing adsorption (SSA). Using quantitative NMR spectroscopy, we demonstrated that electrolyte pH influences CO_2 speciation in electrolyte-soaked electrodes. The NMR methodology allowed us to directly quantify CO_2-speciation within electrolyte-soaked electrodes and provides experimental confirmation of how these equilibria manifest in porous carbon environments across a range of different electrolyte pH values. We find that electrochemical CO_2 uptake occurs in both strongly basic and strongly acidic electrolytes ($pH_{initial}$), even in environments where certain dissolved CO_2 species are expected to be less prevalent. Basic systems containing only bicarbonate showed higher electrochemical adsorption rates than acidic systems that lacked bicarbonate. However, the presence of molecular CO_2 may also play a role in the mechanism, as the highest adsorption capacities were observed in a system containing both CO_2 and bicarbonate (specifically, a basic Na_2SO_4 electrolyte), rather than in the system with the highest bicarbonate concentration (1 M NaOH). These results suggest that electrochemical CO_2 capture by supercapacitors involves mixed contributions from both ionic and molecular liquid–solid mechanisms and can also be explained by a "pH-swing" mechanism.[28,29] Additionally, we found that electrochemical CO_2 adsorption capacity does not correlate with electrochemical capacitance, highlighting the importance of CO_2 speciation in the electrolyte for better understanding the mechanisms of SSA. This study emphasises the critical role of CO_2 speciation in both the mechanism and the performance of SSA. Taken together, our observations suggest that the balance of CO_2-related species and the electrolyte pH can strongly influence electrochemical CO_2 capture performance in aqueous supercapacitor systems. Our work highlights the central role of electrolyte pH in SSA. While further studies are needed to resolve the underlying processes, this work provides new experimental evidence to guide the design of improved capture devices.

Materials and methods

Carbon electrode fabrication

Electrodes were prepared by mixing commercially available activated carbon YP80F (200 mg, Kuraray) with

polytetrafluoroethylene (PTFE) binder (17.5 mg, 60 wt% dispersion in H_2O, Sigma-Aldrich) in a 95 : 5 weight ratio. The carbon and the PTFE were dispersed in ethanol (*ca.* 5 mL, VWR Chemicals) and stirred by hand on a watch glass for 20 min until a jelly-like consistency was achieved. The resulting black material was kneaded with a spatula for 5 min, with ethanol droplets added from time to time to prevent it from drying out. The solid was placed on a glass sheet and rolled out to produce a free-standing carbon electrode (0.25 mm thickness). The electrode thin film was transferred onto aluminium foil and dried in a vacuum oven at 90 °C for 48 hours.

Electrolyte preparation

After initial preparation of neutral (pH_{inital} 7.0) 1 M Na_2SO_4 electrolyte, an acidic ($pH_{initial}$ 1.1) electrolyte was prepared by the combination of 0.17 mL of 1 M H_2SO_4 with 0.2 mL of 1 M Na_2SO_4 electrolyte, and a basic ($pH_{initial}$ 13.4) electrolyte was prepared by combination of 0.07 mL of 1 M NaOH with 0.2 mL of 1 M Na_2SO_4 electrolyte. Electrolyte pH was measured using a pH probe, calibrated using commercial buffers.

10 mL of 1 M $NaHCO_3$ electrolyte was prepared by dissolving 0.84 g of $NaHCO_3$ in a 10 mL volumetric flask and filling the flask to the mark with DI water. For the experiments, 0.2 mL of electrolyte was used to prepare the coin cell.

Meshed coin cell assembly

Two mass-identical carbon electrodes (0.5 inch diameter, 12–15 mg mass range) and glass fibre separators (5/8 inch diameter, GF/A Whatman) were cut with a steel punch. The meshed coin cell was assembled as follows from bottom to top: bottom case, conical spring, spacers (0.5 mm), bottom electrode, separators, 100 μL of electrolyte, gas-exposed electrode and meshed top case (SS316, CR2032, Cambridge Energy Solutions). The coin cell was sealed in a Compact Hydraulic Coin Cell Crimper (Cambridge Energy Solutions) at 80 kg cm^{-2}. The assembled coin cell was then placed inside the gas cell with the meshed side facing the gas reservoir (Fig. 1a).

Meshed coin cell disassembly and pH_{final} estimations

To estimate the pH_{final} of the electrolyte in our gas cells a new set of symmetric coin cell type supercapacitors were assembled using the electrolytes with different $pH_{initals}$. The mass of the carbon electrodes ranged between 10–12 mg and a total of 0.2 mL of electrolyte was added. The cells were sealed and exposed to a pure CO_2 gas reservoir (partial pressure between 0.9–1.1 bar) within the custom made gas cells for 12 h to establish the conditions of SSA measurements. The coin cells were then opened using a coin cell decrimping unit (Cambridge Energy Solutions), the electrolyte was collected from the separator and activated carbon electrodes and the pH_{final} was measured using a pH probe.

Carbon dioxide dosing

To dose the gas reservoir with CO_2 (99.80% purity, BOC), a custom gas manifold was used. The cell was exposed to a static vacuum to avoid evaporation of the electrolyte by opening the two valves on the gas cell. The gas cell pressure dropped to approximately 0.4 bar. In a next step, the valve closest to the cell was closed and the gas manifold was dosed with CO_2 at 1.3 bar. Upon opening the valve to the cell, the CO_2 in the gas manifold mixes with the gas in the reservoir due to the reduced pressure in the gas cell. The valve was closed again and the manifold put back under dynamic vacuum. The dosing process was repeated for a total of 5 cycles to give a 98.7% CO_2 headspace assuming ideal gas mixing.

Pressure measurement

The gas adsorption and desorption was measured with a pressure transducer (PX309-030A5V, Omega). The noise of the pressure transducer is at the level of 0.1 mbar, with a signal to noise ratio of over 5, indicating a reasonable sensitivity of the pressure sensor. For both, the negative and the positive charging protocol, the pressure data was smoothed over 100 seconds. For gas uptake calculations from the pressure data, sudden pressure increases from opening the incubator ovens (temperature drop) were excluded from the analysis.

Electrochemical measurement

A potentiostat (VSP-3e and VMP-3e, Biologic) was used to measure galvanostatic charge and discharge (GCD) and cyclic voltammetry. The gas cell was allowed to reach 30 °C in an incubator oven (SciQuip Incu-80S) to maintain a constant temperature during the measurement. Then the supercapacitor was precycled by conducting 20 cyclic voltammetry cycles at a scan speed of 1 mVs^{-1} within the voltage range of −0.8 V to +0.8 V to activate the electrode–electrolyte interface. In this work, negative and positive charging protocols were applied to conduct the SSA experiments. The supercapacitors were charged to −0.8 V at constant current, the cell voltage was held at −0.8 V for 5 min, then the supercapacitor was discharged back to 0 V again, and the cell voltage was held for another 5 min at 0 V. This protocol was also applied for the positive charging mode.

ss-NMR measurements

Solid-state NMR sample preparation and measurement was carried out per the method described previously in Coady *et al.* (2025),[30] with minor adjustments detailed below.

Activated carbon films were cut into small pieces, then an approximately 10 mg sample was weighed and placed in a vial. Electrolyte (either pH initial 1.1, pH initial 7.0, or pH initial 13.4 1 M $Na_2SO_{4(aq)}$, or 1 M $NaOH_{(aq)}$) was then added to achieve a 2 : 3 mass/volume ratio of activated carbon and electrolyte. The vial was sealed and left for 5 minutes to allow electrolyte to saturate the sample. Then, the electrolyte-soaked electrode was packed into a 3.2 mm rotor as quickly as possible to minimize evaporation of the solvent. Samples and vessels were weighed before and after addition of solvent and packing to quantify any loss of solvent due to evaporation.

Each sample was briefly evacuated for 1 minute under a static vacuum in a home-built gas manifold, as described

previously in Forse *et al.* 2018.[46] Samples were then dosed with $^{13}CO_{2(g)}$ at a pressure of 0.7 bar for 30 minutes, before rotors were sealed while inside the gas manifold using a mechanical plunger.

The NMR experiments were carried out using a Bruker Avance Neo spectrometer in a Bruker 3.2 mm HXY triple resonance probe. For the measurements, a magnetic field strength of 9.4 T was applied, corresponding to a ^{1}H Larmor frequency of 400.1 MHz. All spectra were acquired with a 90° pulse-acquire sequence at an MAS speed of 5 kHz, at which speed we observe resolved spectra while avoiding excess frictional heating or centrifugation.[47,48] The 90° pulse length was optimised for every sample. Recycle delays were set to >5 T_1 for the CO_2 and the HCO_3^- peaks for each sample to guarantee a quantitative measurement. T_1 was measured through inversion recovery experiments. The ^{13}C NMR spectra were referenced relative to the ^{13}C CH resonance of adamantane at 37.78 ppm as a secondary reference to TMS. NMR spectra were processed and integrated using the Topspin software and Python code. A full description of the data analysis procedure is described in the SI.

Point of zero charge measurements (PZC)

The point of zero charge (PZC) was performed using the pH drift method. For the measurement, 60 mg of cut activated carbon thin film was added to 500 μL of aqueous Na_2SO_4 electrolyte at different pH values. The carbon suspension was left overnight to reach equilibrium. The electrolyte pH was measured using a calibrated pH meter (Mettler Toledo). The PZC was determined graphically by the intercept between the pH sorption plateau and the line through the origin with a slope of 1 (equivalent to no ion adsorption).

Author contributions

A. C. F., Z. C. and Z. X. supervised and guided the project. All authors designed the research. S. E. W. prepared the electrode and electrolyte fabrication, device assembly, electrochemical CO_2 capture testing and data analysis. Z. C. conducted the solid-state NMR experiments and analysed the results. S. E. W. and Z. C. drafted the manuscript and all authors contributed to the manuscript revision.

Conflicts of interest

The authors declare no competing interests.

Data availability

All raw experimental data files are available in the Cambridge Research Repository, Apollo, with the identifier: https://doi.org/10.17863/CAM.129151.

Supplementary information (SI) is available. See DOI: https://doi.org/10.1039/d5ta10332k.

Acknowledgements

The authors thank Cerys Walsh, Dr Grace Mapstone, and Trevor Binford for invaluable scientific discussions. This work was supported by a UKRI Future Leaders Fellowship to A. C. F. (MR/T043024/1, and MR/Y034244/1). Z. C. acknowledges the Gates Cambridge Trust for its support.

References

1 K. Rennert, F. Errickson, B. C. Prest, L. Rennels, R. G. Newell, W. Pizer, C. Kingdon, J. Wingenroth, R. Cooke, B. Parthum, D. Smith, K. Cromar, D. Diaz, F. C. Moore, U. K. Müller, R. J. Plevin, A. E. Raftery, H. Ševčíková, H. Sheets, J. H. Stock, T. Tan, M. Watson, T. E. Wong and D. Anthoff, Comprehensive Evidence Implies a Higher Social Cost of CO2, *Nature*, 2022, **610**(7933), 687–692, DOI: 10.1038/s41586-022-05224-9.

2 V. Masson-Delmotte; H.-O. Pörtner; J. Skea; P. Zhai; D. Roberts; P. R. Shukla; Group, I. P. on C. C. R. S. W.; Group, I. P. on C. C. I. W.; I, I. P. on C. C. W. G.; Inventories, I. P. on C. C. T. F. on N. G. Global Warming of 1.5 °C. 2019.

3 S. Pye, F. G. N. Li, J. Price and B. Fais, Achieving Net-Zero Emissions through the Reframing of UK National Targets in the Post-Paris Agreement Era, *Nat. Energy*, 2017, **2**(3), 1–7, DOI: 10.1038/nenergy.2017.24.

4 J. E. Hansen, P. Kharecha, M. Sato, G. Tselioudis, J. Kelly, S. E. Bauer, R. Ruedy, E. Jeong, Q. Jin, E. Rignot, I. Velicogna, M. R. Schoeberl, K. von Schuckmann, J. Amponsem, J. Cao, A. Keskinen, J. Li and A. Pokela, Global Warming Has Accelerated: Are the United Nations and the Public Well-Informed?, *Environ. Sci. Policy Sustain. Dev.*, 2025, **67**(1), 6–44, DOI: 10.1080/00139157.2025.2434494.

5 H.-J. Ho, A. Iizuka and E. Shibata, Carbon Capture and Utilization Technology without Carbon Dioxide Purification and Pressurization: A Review on Its Necessity and Available Technologies, *Ind. Eng. Chem. Res.*, 2019, **58**(21), 8941–8954, DOI: 10.1021/acs.iecr.9b01213.

6 F. Meng, Y. Meng, T. Ju, S. Han, L. Lin and J. Jiang, Research Progress of Aqueous Amine Solution for CO2 Capture: A Review, *Renew. Sustain. Energy Rev.*, 2022, **168**, 112902, DOI: 10.1016/j.rser.2022.112902.

7 S. E. Renfrew, D. E. Starr and P. Strasser, Electrochemical Approaches toward CO2 Capture and Concentration, *ACS Catal*, 2020, **10**(21), 13058–13074, DOI: 10.1021/acscatal.0c03639.

8 R. A. Shaw and T. A. Hatton, Electrochemical CO2 Capture Thermodynamics, *Int. J. Greenh. Gas Control*, 2020, **95**, 102878, DOI: 10.1016/j.ijggc.2019.102878.

9 J. Taylor, A. Forse and A. Thom, Impacts of Quinone Structure on Trade-Offs Between Redox Potential and CO2 Binding Strength, *ChemPhysChem*, 2026, **27**, e202500472, DOI: 10.1002/cphc.202500472.

10 Y. Jing, K. Amini, D. Xi, S. Jin, A. M. Alfaraidi, E. F. Kerr, R. G. Gordon and M. J. Aziz, Electrochemically Induced

CO2 Capture Enabled by Aqueous Quinone Flow Chemistry, *ACS Energy Lett*, 2024, **9**(7), 3526–3535, DOI: 10.1021/acsenergylett.4c01235.

11 P. Śledzik, P. M. Biesheuvel, Q. Shu, H. V. M. Hamelers and S. Porada, Continuous Electrochemical Carbon Capture via Redox-Mediated pH Swing—Experimental Performance and Process Modeling, *J. Phys. Chem. Lett.*, 2025, **16**(5), 1343–1351, DOI: 10.1021/acs.jpclett.4c03111.

12 R. Sharifian, R. M. Wagterveld, I. A. Digdaya, C. Xiang and D. A. Vermaas, Electrochemical Carbon Dioxide Capture to Close the Carbon Cycle, *Energy Environ. Sci.*, 2021, **14**(2), 781–814, DOI: 10.1039/D0EE03382K.

13 B. Kokoszka, N. K. Jarrah, C. Liu, D. T. Moore and K. Landskron, Supercapacitive Swing Adsorption of Carbon Dioxide, *Angew. Chem., Int. Ed.*, 2014, **53**(14), 3698–3701, DOI: 10.1002/anie.201310308.

14 Poonam, K. Sharma, A. Arora and S. K. Tripathi, Review of Supercapacitors: Materials and Devices, *J. Energy Storage*, 2019, **21**, 801–825, DOI: 10.1016/j.est.2019.01.010.

15 F. ulH. Khan, M. Bilal, J. Li, X. Xu and K. Landskron, Supercapacitive Swing Adsorption of CO2: Advances and Future Prospects, *Trends Chem*, 2025, **7**(1), 43–55, DOI: 10.1016/j.trechm.2024.11.003.

16 P. Zhu, Z.-Y. Wu, A. Elgazzar, C. Dong, T.-U. Wi, F.-Y. Chen, Y. Xia, Y. Feng, M. Shakouri, J. Y. Kim, Z. Fang, T. A. Hatton and H. Wang, Continuous Carbon Capture in an Electrochemical Solid-Electrolyte Reactor, *Nature*, 2023, **618**(7967), 959–966, DOI: 10.1038/s41586-023-06060-1.

17 T. B. Binford, G. Mapstone, I. Temprano and A. C. Forse, Enhancing the Capacity of Supercapacitive Swing Adsorption CO_2 Capture by Tuning Charging Protocols, *Nanoscale*, 2022, **14**(22), 7980–7984, DOI: 10.1039/D2NR00748G.

18 S. Zhu, J. Li, A. Toth and K. Landskron, Relationships between the Elemental Composition of Electrolytes and the Supercapacitive Swing Adsorption of CO2, *ACS Appl. Energy Mater.*, 2019, **2**(10), 7449–7456, DOI: 10.1021/acsaem.9b01435.

19 S. Zhu, J. Li, A. Toth and K. Landskron, Relationships between Electrolyte Concentration and the Supercapacitive Swing Adsorption of CO2, *ACS Appl. Mater. Interfaces*, 2019, **11**(24), 21489–21495, DOI: 10.1021/acsami.9b03598.

20 Z. Xu, G. Mapstone, Z. Coady, M. Wang, T. L. Spreng, X. Liu, D. Molino and A. C. Forse, Enhancing Electrochemical Carbon Dioxide Capture with Supercapacitors, *Nat. Commun.*, 2024, **15**(1), 7851, DOI: 10.1038/s41467-024-52219-3.

21 Y. Wang, X. Sun, K. Zhang, J. Feng, X. Sun, C. Li, K. Wang, X. Zhang and Y. Ma, Effects of Activated Carbon Types on the CO2 Supercapacitive Swing Adsorption Performances, *J. Solid State Electrochem.*, 2025, **30**, 17–30, DOI: 10.1007/s10008-025-06271-8.

22 M. Bilal, J. Li and K. Landskron, Enhancing Supercapacitive Swing Adsorption of CO2 with Advanced Activated Carbon Electrodes, *Adv. Sustain. Syst.*, 2023, **7**(11), 2300250, DOI: 10.1002/adsu.202300250.

23 M. Bilal, J. Li, H. Guo and K. Landskron, High-Voltage Supercapacitive Swing Adsorption of Carbon Dioxide, *Small*, 2023, **19**(24), 2207834, DOI: 10.1002/smll.202207834.

24 S. Zhu, K. Ma and K. Landskron, Relationships between the Charge–Discharge Methods and the Performance of a Supercapacitive Swing Adsorption Module for CO2 Separation, *J. Phys. Chem. C*, 2018, **122**(32), 18476–18483, DOI: 10.1021/acs.jpcc.8b03968.

25 Z. Xu, X. Liu, G. Mapstone, Z. Coady, C. Seymour, S. Wiesner, S. Menkin and A. Forse, Breaking Supercapacitor Symmetry Enhances Electrochemical Carbon Dioxide Capture, *J. Am. Chem. Soc.*, 2025, **147**, 16189–16197, DOI: 10.1021/jacs.5c00999.

26 G. Mapstone, T. M. Kamsma, Z. Xu, P. K. Jones, A. A. Lee, I. Temprano, J. Lee, M. F. L. De Volder and A. C. Forse, Understanding the Mechanism of Electrochemical CO2 Capture by Supercapacitive Swing Adsorption, *ACS Nano*, 2025, **19**, 4242–4250, DOI: 10.1021/acsnano.4c10931.

27 R. Ding, A.-R. Siddiqui, K. Martin, J. N'Diaye, J. B. Varley, J. Dawlaty, J. Rodríguez-López and V. Augustyn, Dissolved CO2 Modulates the Electrochemical Capacitance on Gold Electrodes, *ACS Electrochem*, 2025, **1**, 476–485, DOI: 10.1021/acselectrochem.4c00098.

28 K. Sun, M. Tebyetekerwa, H. Zhang, R. Evans, L. Ge, Y. Sun, Y. Ge, Z. Wang, C. Xing, J. Yang, X. Zeng, D. Martin and X. Zhang Membrane-Separated Electrodes Enable High-Rate Low Energy Electrochemical Carbon Capture, *ChemRxiv*, 2025, preprint, DOI: 10.26434/chemrxiv-2025-9pmwf-v2.

29 F. Khan and K. Landskron Mechanistic Insights into Supercapacitive Swing Adsorption via Acid-Base Titrations. *ChemRxiv*, 2025, preprint, DOI: 10.26434/chemrxiv-2025-vl4dh.

30 Z. Coady, S. G. H. Brookes, Z. Shen, B. J. Rhodes, G. Mapstone, Z. Xu, W. Yu, H. Nishihara, C. Schran, A. Michaelides and A. C. Forse, Unexpected Oversolubility of CO2 Measured at Electrode–Electrolyte Interfaces, *J. Am. Chem. Soc.*, 2025, **147**(40), 36310–36319, DOI: 10.1021/jacs.5c09712.

31 D. Lyu, K. Märker, Y. Zhou, E. W. Zhao, A. B. Gunnarsdóttir, S. P. Niblett, A. C. Forse and C. P. Grey, Understanding Sorption of Aqueous Electrolytes in Porous Carbon by NMR Spectroscopy, *J. Am. Chem. Soc.*, 2024, **146**(14), 9897–9910, DOI: 10.1021/jacs.3c14807.

32 N. Dasgupta, T. A. Ho, S. B. Rempe and Y. Wang, Effects of Surface Hydrophilicity and Heterogeneity on CO2 Conversion to H2CO3 in the Nanopores of Layered Materials, *J. Phys. Chem. C*, 2024, **128**(14), 5878–5888, DOI: 10.1021/acs.jpcc.3c08383.

33 R. Vieira, I. Marin-Montesinos, J. Pereira, R. Fonseca, M. Ilkaeva, M. Sardo and L. Mafra, Hidden" CO_2 in Amine-Modified Porous Silicas Enables Full Quantitative NMR Identification of Physi- and Chemisorbed CO_2 Species, *J. Phys. Chem. C*, 2021, **125**(27), 14797–14806, DOI: 10.1021/acs.jpcc.1c02871.

34 L. Mafra, T. Čendak, S. Schneider, P. V. Wiper, J. Pires, J. R. B. Gomes and M. L. Pinto, Structure of Chemisorbed

CO2 Species in Amine-Functionalized Mesoporous Silicas Studied by Solid-State NMR and Computer Modeling, *J. Am. Chem. Soc.*, 2017, **139**(1), 389–408, DOI: 10.1021/jacs.6b11081.

35 T. M. Abbott, G. W. Buchanan, P. Kruus and K. C. Lee, 13C Nuclear Magnetic Resonance and Raman Investigations of Aqueous Carbon Dioxide Systems, *Can. J. Chem.*, 1982, **60**(8), 1000–1006, DOI: 10.1139/v82-149.

36 H. Li, M. E. Zick, T. Trisukhon, M. Signorile, X. Liu, H. Eastmond, S. Sharma, T. L. Spreng, J. Taylor, J. W. Gittins, C. Farrow, S. A. Lim, V. Crocellà, P. J. Milner and A. C. Forse, Capturing Carbon Dioxide from Air with Charged-Sorbents, *Nature*, 2024, **630**(8017), 654–659, DOI: 10.1038/s41586-024-07449-2.

37 C. Perinu, B. Arstad and K.-J. Jens, 13C NMR Experiments and Methods Used to Investigate Amine-CO2-H2O Systems, *Energy Procedia*, 2013, **37**, 7310–7317, DOI: 10.1016/j.egypro.2013.06.669.

38 F. Mani, M. Peruzzini and P. Stoppioni, CO2 Absorption by Aqueous NH3 Solutions: Speciation of Ammonium Carbamate, Bicarbonate and Carbonate by a 13C NMR Study, *Green Chem*, 2006, **8**(11), 995–1000, DOI: 10.1039/B602051H.

39 E. H. Lahrar and C. Merlet, Investigating the Effect of Particle Size Distribution and Complex Exchange Dynamics on NMR Spectra of Ions Diffusing in Disordered Porous Carbons through a Mesoscopic Model, *Faraday Discuss*, 2025, **255**, 355–369, DOI: 10.1039/D4FD00082J.

40 E. G. Calvo, N. Rey-Raap, A. Arenillas and J. A. Menéndez, The Effect of the Carbon Surface Chemistry and Electrolyte pH on the Energy Storage of Supercapacitors, *RSC Adv.*, 2014, **4**(61), 32398–32404, DOI: 10.1039/C4RA04430D.

41 H. A. Andreas and B. E. Conway, Examination of the Double-Layer Capacitance of an High Specific-Area C-Cloth Electrode as Titrated from Acidic to Alkaline pHs, *Electrochim. Acta.*, 2006, **51**(28), 6510–6520, DOI: 10.1016/j.electacta.2006.04.045.

42 B. E. Conway, *Electrochemical Supercapacitors*, Springer US, Boston, MA, 1999, DOI: 10.1007/978-1-4757-3058-6.

43 Y. Chen, Q. Dou, J. Yang, C. Huang, P. Tang, S. Xue, A. Tang, X. Yu, Y. Cao and X. Yan, CO2-Regulated, Ultrahigh-Concentration Aqueous Electrolytes for High Energy and Power of Supercapacitors, *Chem. Eng. J.*, 2024, **496**, 154007, DOI: 10.1016/j.cej.2024.154007.

44 M. Liu, Y.-L. Wang, K. Schutjajew, L. Chai and M. Oschatz, Ion Bridging by Carbon Dioxide Facilitates Electrochemical Energy Storage at Charged Carbon–Ionic–Liquid Interfaces, *Adv. Energy Mater.*, 2023, **13**(21), 2300401, DOI: 10.1002/aenm.202300401.

45 X. Wang, A. Y. Mehandzhiyski, B. Arstad, K. L. Van Aken, T. S. Mathis, A. Gallegos, Z. Tian, D. Ren, E. Sheridan, B. A. Grimes, D. Jiang, J. Wu, Y. Gogotsi and D. Chen, Selective Charging Behavior in an Ionic Mixture Electrolyte-Supercapacitor System for Higher Energy and Power, *J. Am. Chem. Soc.*, 2017, **139**(51), 18681–18687, DOI: 10.1021/jacs.7b10693.

46 A. C. Forse, P. J. Milner, J.-H. Lee, H. N. Redfearn, J. Oktawiec, R. L. Siegelman, J. D. Martell, B. Dinakar, L. B. Zasada, M. I. Gonzalez, J. B. Neaton, J. R. Long and J. A. Reimer, Elucidating CO2 Chemisorption in Diamine-Appended Metal–Organic Frameworks, *J. Am. Chem. Soc.*, 2018, **140**(51), 18016–18031, DOI: 10.1021/jacs.8b10203.

47 A. C. Forse, J. M. Griffin, C. Merlet, P. M. Bayley, H. Wang, P. Simon and C. P. Grey, NMR Study of Ion Dynamics and Charge Storage in Ionic Liquid Supercapacitors, *J. Am. Chem. Soc.*, 2015, **137**(22), 7231–7242, DOI: 10.1021/jacs.5b03958.

48 L. M. Dickinson, R. K. Harris, J. A. Shaw, M. Chinn and P. R. Norman, Oxygen-17 and Deuterium NMR Investigation into the Adsorption of Water on Activated Carbon, *Magn. Reson. Chem.*, 2000, **38**(11), 918–924, DOI: 10.1002/1097-458X(200011)38:11<918::AID-MRC749>3.0.CO;2-7.